Synthesis and Investigation of Pure and Cu-Doped NiO Nanofilms for Future Applications in Wastewater Treatment Rejected by Textile Industry

Malika Allali, Mohamed Amine Dahamni, Mostefa Ghamnia, Abdelwahab Boukhachem, Djamel Boukrédimi, Didier Tonneau, Carole Fauquet

catalysts

MDPI

Article

Synthesis and Investigation of Pure and Cu-Doped NiO Nanofilms for Future Applications in Wastewater Treatment Rejected by Textile Industry

Malika Allali [1], Mohamed Amine Dahamni [1], Mostefa Ghamnia [1,*], Abdelwahab Boukhachem [2], Djamel Boukrédimi [3], Didier Tonneau [4] and Carole Fauquet [4]

[1] Laboratoire des Sciences de la Matière Condensée (LSMC), Université Oran 1 Ahmed Ben Bella, Oran 31100, Algeria
[2] Laboratoire de Nanomatériaux et Systèmes pour Energies Renouvelables, Centre de Recherches et des Technologies de l'Energie, Technopôle de Borj-Cédria, BP 95 Hammam-Lif, Tunis 2050, Tunisia
[3] Institut des Sciences et Techniques Appliquées (ISTA), Université Oran 1 Ahmed ben Bella, Oran 31100, Algeria
[4] Centre Interdisciplinaire de Nanosciences de Marseille (CINaM), CNRS, Aix Marseille Université, 13288 Marseille, France
* Correspondence: mghamnia@yahoo.fr

Abstract: Pure and Cu-doped NiO films were synthesized via a soft chemical process. They were deposited on glass substrates heated to 400 °C. Different atomic percentage ratios (2, 4, 6, 8, and 10%) of Cu-doping were used. The prepared samples were characterized by several techniques such as X-ray diffraction for crystallographic study, SEM and AFM for microstructural and morphological properties, and UV-Visible spectroscopy for optical and photocatalytical analysis. XRD results of pure and Cu-doped NiO films indicated the formation of NiO polycrystalline phases under a cubic structure with a favored orientation along the (200) plane noticed in all sprayed films. SEM images revealed the formation of NiO nanoparticles of spherical forms whose sizes increase and agglomerate with increasing Cu-doping. At 10% Cu-doping, NiO agglomeration was extended to the whole surface. AFM images showed a textured and rough surface composed of NiO nanoparticles of average size varying from 16 to 10 nm depending on Cu-doping concentration. UV-visible spectroscopy confirmed the transparency of NiO films and their semiconducting character with a band gap ranging from 3.4450 eV to 2.8648 eV. The photocatalytical properties of pure and Cu-NiO films were enhanced by Cu-doping particles as revealed by the degradation of methylene blue (MB) solution subjected to irradiation.

Keywords: NiO synthesis; spray pyrolysis; Cu-doping; nanograins; photocatalytic properties

Citation: Allali, M.; Dahamni, M.A.; Ghamnia, M.; Boukhachem, A.; Boukrédimi, D.; Tonneau, D.; Fauquet, C. Synthesis and Investigation of Pure and Cu-Doped NiO Nanofilms for Future Applications in Wastewater Treatment Rejected by Textile Industry. *Catalysts* **2022**, *12*, 931. https://doi.org/10.3390/catal12090931

Academic Editor: John Vakros

Received: 31 July 2022
Accepted: 15 August 2022
Published: 23 August 2022

1. Introduction

Transparent Conducting Oxides (TCO) such as ZnO, TiO_2, SnO_2, CuO, etc., continue to receive considerable attention due to their outstanding electrical, magnetic, and catalytic properties [1–4]. They are essential compounds for the development of ultra-high frequency components, gas sensors, optoelectronics, and batteries [5–7]. As the textile industries are disposing of unused direct dyes into the aquatic environment, which is posing a serious, alarming threat to aquatic life, recent studies are increasingly interested in wastewater treatment because the nanofilms of these materials allow the photodegradation of dyes rejected by the textile industry [8–11].

As a reminder, dyes are aromatic organic compounds which have the property of absorbing light and giving color in the visible region. This important property is exploited in many industries such as textiles, food, cosmetics, medicine, etc., which generate a huge amount of wastewater containing toxic dyes that pollute the environment. Among the various dyestuffs, methylene blue (MB) is the most commonly used in the textile industry

for coloring silk, wool, cotton, etc., but MB, contained in the wastewater discharged by the textile industry, is toxic and carcinogenic. It is non-biodegradable and can cause a severe threat to human health and environmental safety. Textile industries release significant amounts of MB dyes into natural water sources, which is a threat to public health because of the toxicity of MB, which becomes harmful above a certain concentration [12,13].

Therefore, photocatalysis stands out as one methodology that can be effectively exploited for the complete mineralization of various dye pollutants present in wastewater. Photodegradation is an advanced oxidation process which is used in this work for MB removal.

Currently, nickel oxide (NiO) nanoparticles are particularly attracting the attention of the scientific community [14–16] for its use in this domain. NiO is one of the parts of this family of TCO; it is known for its good adsorptive properties and chemical stability. NiO is one of the p-type semiconductor materials with an optical band gap ranging from 3.6 to 4.0 eV [17,18] and has a wide range of applications, such as gas sensors, photocatalysis, dye-sensitized, electrochromic coatings, UV photodetector, lightweight structural components in the aerospace, in ceramic structures, a counter electrode and anode layer of solid, and counter electrodes oxide fuel cells [19–23]. However, most of these applications require particles with a small size and a narrow size distribution. With the volume effect, the quantum size effect, and the surface effect, NiO nanoparticles are expected to possess many improved properties and even more attractive applications than those of bulk-sized NiO particles.

NiO nanofilms containing nanoparticles can be produced by several physical and chemical techniques such as reactive evaporation, molecular beam epitaxy (MBE), magnetron sputtering technique, pulsed laser deposition (PLD), spray pyrolysis, sol–gel process, chemical vapor deposition, and electrochemical deposition [24–26]. Among these methods, spray deposition has many advantages, such as low cost, simple deposition equipment, easy fabrication of large-area films, easier adjustment of composition, and being able to carry out doping at the molecular level.

The spray pyrolysis method, which gave good results in previous works [27–29], was used here to synthesize NiO nanofilms from Nickel (II) nitrate hexahydrate ($(Ni(NO_3)_2{\cdot}6H_2O)$ as the inorganic precursor. We also investigated the influence of copper (Cu) doping on the quality of NiO films. All deposits were made on glass substrates heated to 400 °C. Investigation and characterization of structural, optical, and photocatalytical properties of prepared NiO nanofilms were performed using X-ray diffraction, scanning electron microscopy (SEM), atomic force microscopy (AFM) and UV-visible spectroscopy.

2. Results and Discussion

2.1. Structural and Morphological Properties

2.1.1. XRD Characterization

In Figure 1, we report the X-ray diffractograms of pure NiO thin films and copper-doped NiO with doping ratios of 2, 4, 6, 8, and 10%. As a first result, all films showed well-defined peaks with orientations in the (111), (200), (220), (311), (222), and (400) crystal planes which correspond to 2θ diffraction angles around 37.01°, 42.95°, 62.65°, 75.25°, 78.94°, and 94.75°.

The peaks related to (111) and (200) planes are the most shown and discussed in the literature [30–32]. They denote that pure and Cu-NiO thin films are polycrystalline and crystallizes in face-centered cubic. No trace of impurity is observed on these diffractograms, this shows the high-purity of the nickel oxide deposits. All Cu-NiO films displayed only NiO peaks, even after adding higher Cu. This may appear unlikely because doping with transition metals decreases always the intensity of XRD peaks. However, because of the ionic radius and electronegativity of Ni^{2+} (r_{Ni2+} = 0.78 Å) and Cu^{2+} (r_{Cu2+} = 0.82 Å) are of same of order ($r_{Cu2+}/r_{Ni2+}/ \approx 1.05$), Cu^{2+} ions can be easily substitute for Ni ions and fill nickel vacancies without significant lattice distortion. This is why Cu-doped NiO displayed typical XRD patterns of NiO in good agreement with the works of Chen et al.

and Gowthami et al. [33,34]. As it can be observed in Figure 1, the peaks are relatively broadened, and the intensity of the (200) diffraction peaks increases with the increase in Cu-doping concentration, indicating the enlacement of particle size due to Cu doping.

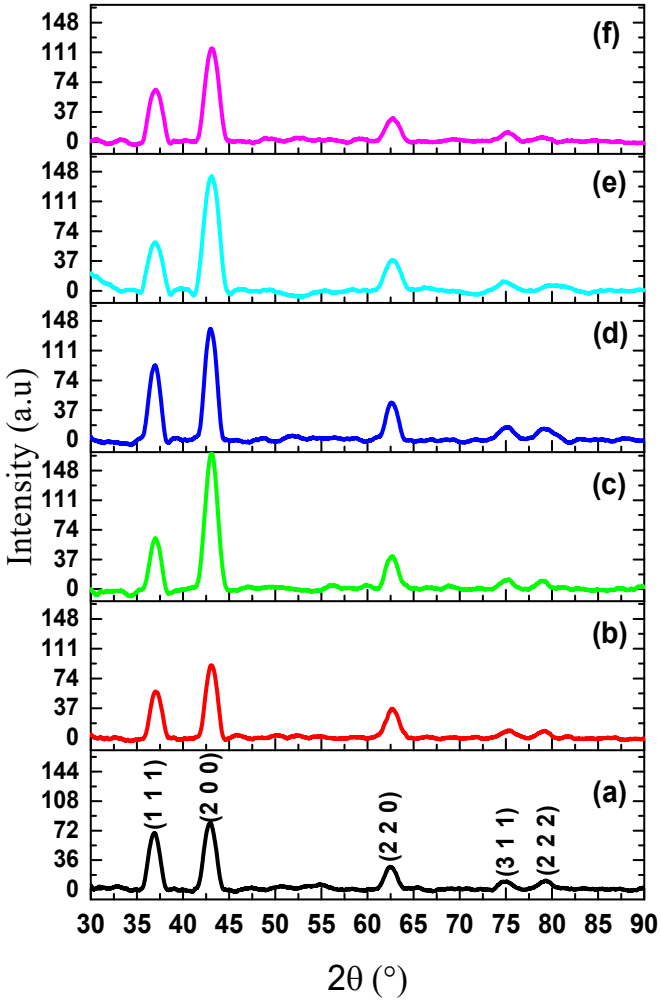

Figure 1. XRD patterns of pure and Cu-doped NiO films. (**a**) Pure NiO, (**b**) 2% Cu-doped NiO, (**c**) 4% Cu-doped NiO, (**d**) 6% Cu-doped NiO, (**e**) 8% Cu-doped NiO, and (**f**) 10% Cu-doped NiO.

From XRD spectra, we can determine the lattice parameters *a*, *b*, and *c* of the deposited films by the relation below. As NiO adopts the NaCl structure, with octahedral Ni^{2+} and O^{2-} sites, the lattice parameters are equal (*a* = *b* = *c*).

$$\frac{1}{d_{hkl}^2} = \frac{h^2 + k^2 + l^2}{a^2} \quad (1)$$

where d_{hkl} is the interplanar spacing determined from Bragg equation [35]:

$$2\, d_{hkl}\, sin\theta = n\, \lambda \quad (2)$$

λ is the wavelength of Cu-Kα radiation (1.54 Å), θ is the diffraction angle, and *n* is the order of diffraction (usually *n* = 1). *a*, *h*, *k*, and *l* in Equation (1) are the lattice parameter and Miller indices, respectively.

The values of the parameter *a* deduced from this relation for the plane (200) for pure and Cu-doped NiO samples are displayed in Table 1.

Table 1. Estimation of lattice parameter.

Samples	2θ	a (Å)	a (Å) from in Literature
Pure NiO	42.93	4.1092	4.1605–4.1787 [36] 4.16–4.19 [37] 4.204 [38]
2% Cu-doped NiO	43.08	4.1952	
4% Cu-doped NiO	43.11	4.1968	
6% Cu-doped NiO	43.00	4.2026	
8% Cu-doped NiO	43.08	4.2066	
10% Cu-doped NiO	43.13	4.2105	

From this table, the values of lattice parameter a vary from 4.1092 to 4.2105 Å from pure to Cu-doped NiO. These values, which vary slightly with Cu-doping, agree well with those performed in the literature for synthesized NiO films [36–38].

The grain sizes of NiO and Cu-NiO crystallites are estimated from the use of the following Debye–Sherrer formula [39]:

$$D = \frac{0.9\lambda}{\beta(2\theta)cos\theta} \quad (3)$$

where λ is the X-ray wavelength, θ is the Bragg diffraction angle, and β is the broadening of the diffraction peak measured at half of its maximum (FWHM) intensity.

The dislocation density δ, which is defined as the number of dislocation lines per unit volume of crystal, depends on the nanoparticles sizes and is calculated using the following formula [40]:

$$\delta = \frac{1}{D^2} \quad (4)$$

Micro-strain (ε), which occurs during growth, is affected by the stretching of the crystal lattice. It is evaluated from the formula [41].

$$\varepsilon = \frac{\beta(2\theta)cos\theta}{4} \quad (5)$$

Table 2 summarizes the values of D, ε, and δ for the most intense (200) diffraction peak.

Table 2. Determination of grain size, micro strain and dislocation density.

Samples	D (nm)	$\varepsilon \times 10^{-3}$	$\delta \times 10^{-3}$
Pure NiO	6.6125	15.3061	22.80
2% Cu-doped NiO	6.4625	14.9092	14.90
4% Cu-doped NiO	6.4274	16.6267	24.20
6% Cu-doped NiO	5.9303	15.3658	28.43
8% Cu-doped NiO	5.5810	18.6885	32.10
10% Cu-doped NiO	5.2737	17.6454	35.95

From the values of this table, the estimated crystallite size was 6.6125 nm for pure NiO, and it decreases with increased Cu-doping. Cu-doping seems to have an effect on the improvement of the crystalline quality by reducing Ni^{2+} vacancies. Micro-strain (ε), which occurs during NiO film growth, depends also on cu-doping. It acts on the compression and on the stretching of the lattice [42]. The dislocation density (δ) decreases with the increase in Cu-doping. Cu-atoms create imperfections in the crystal by the appearance of the lattice displacement between different planes of the crystal [43].

2.1.2. Microstructural Study

The subsurface morphology of NiO nanofilms was studied by scanning electron microscopy (SEM) combined with EDX. EDX giving quantitative chemical composition revealed an equivalent proportion of nickel Ni and oxygen O. From Table 3, the atomic ratio is ≈ 1, which shows that synthesized NiO films are stoichiometric.

Table 3. EDX analysis of chemical species.

Scheme	Ni (% at.)	O (% at.)	Atomic Ratio (Ni/O)	Cu (% at.)
Pure NiO	44.7	48.6	0.91	0
2% Cu-doped NiO	52.1	45.9	1.13	0.1
4% Cu-doped NiO	52	46.3	1.12	0.4
6% Cu-doped NiO	49.8	48	1.03	1.7
8% Cu-doped NiO	47.3	45	1.05	2.9
10% Cu-doped NiO	45.6	44.8	1.01	6.9

Figure 2 shows the distinctive SEM images of pure and Cu- NiO films and their qualitative chemical composition. So as not to clutter the paper, we have chosen only three SEM images corresponding to pure, 6, and 10% Cu-doped NiO. As it can be observed: with increasing Cu-doping, NiO surface is composed of spherical nanoparticles which agglomerate and increase along the surface with cu-doping. At 10% of Cu atoms, the substrate becomes completely covered with NiO particles exhibiting nanoagglomerations continue its formation in becoming microagglomerations.

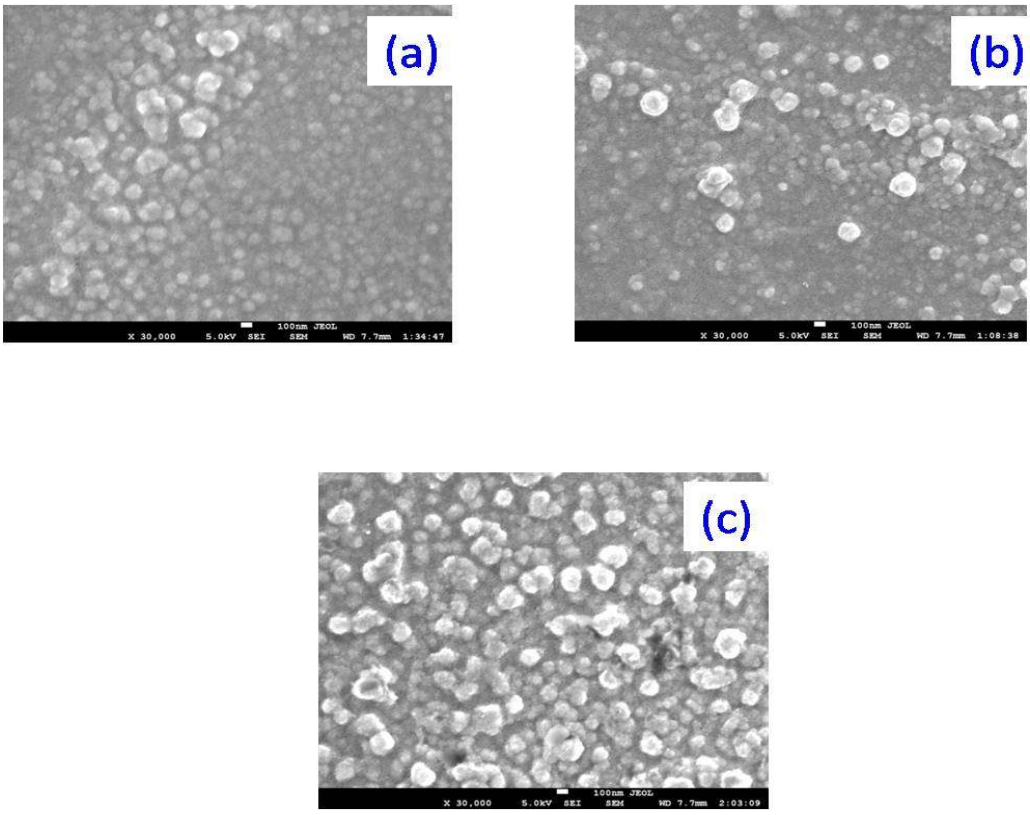

Figure 2. SEM images Evolution the NiO microstructure with Cu-doping. (**a**) Pure NiO, (**b**) 6% Cu-NiO, and (**c**) 10% Cu-NiO.

2.1.3. AFM Characterization

AFM images of undoped and Cu-doped niO films with different Cu contents are shown in Figure 3. As in SEM, we reported only AFM images for pure, 6, and 10% Cu-NiO. The AFM topography of the as-deposited NiO films prepared reveals that the film surface is rather textured and rough. AFM observations show clear grains whose size depends on Cu-doping.

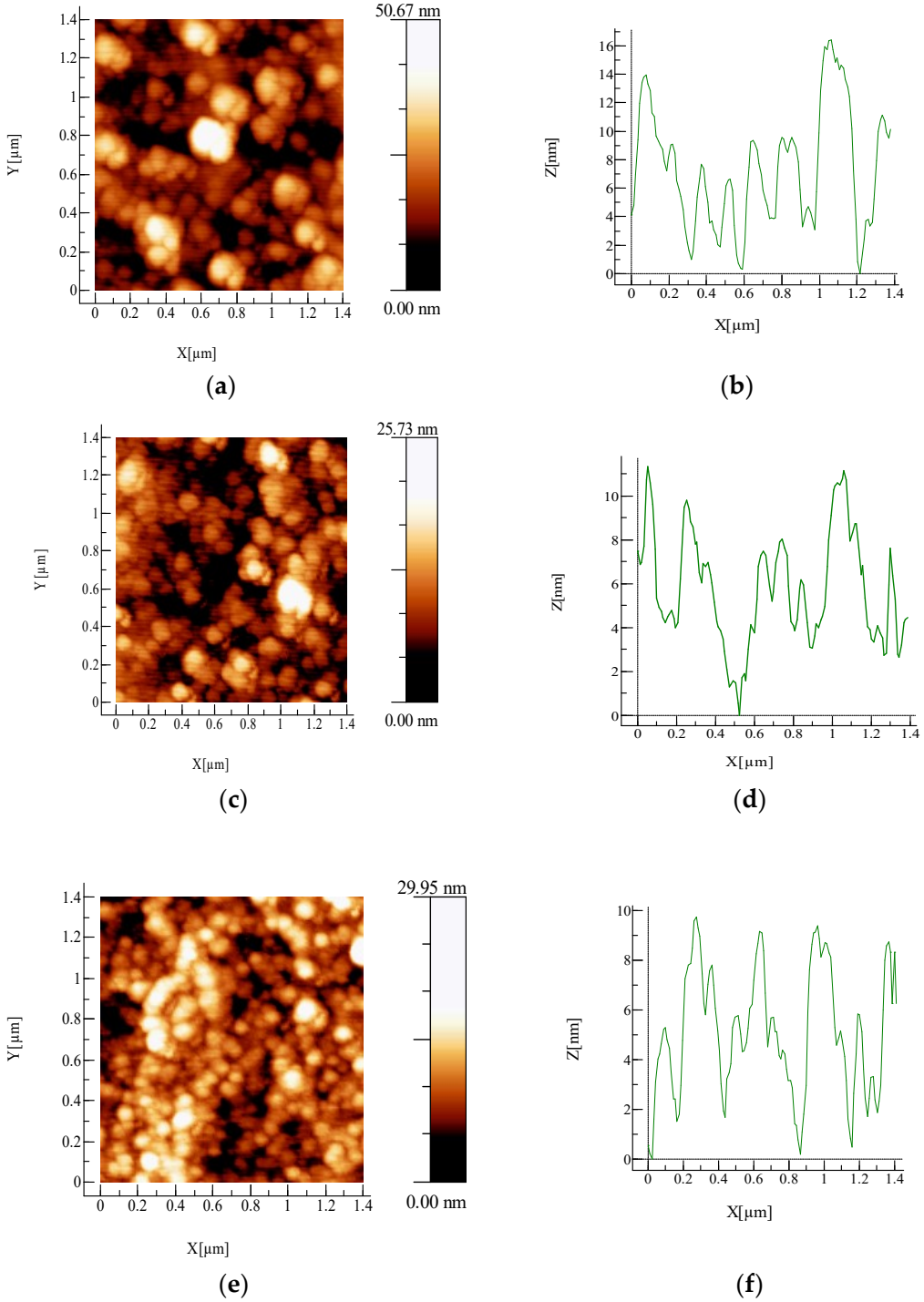

Figure 3. AFM images (**a**): Pure NiO, (**c**) 6% Cu-NiO, (**e**) 10% Cu-NiO; (**b**,**d**,**f**): profile showing the evolution of pure NiO, 6%, and 10% Cu-NiO film surfaces.

According to the profile plotted on the right of the AFM images, the average size of pure NiO nanoparticles is greater than 16 nm, while it is 14 and 10 nm for pure, 6, and 10% Cu-NiO, respectively. As discussed in the XRD paragraph, the decreased NiO nanoparticles size with Cu-doping improves the crystalline quality.

2.2. Optical Properties

In order to determine the effect of Cu-doping on the optical properties, transmittance spectra were measured by using UV-visible spectrometry in a double-beam spectrophotometer operated in the wavelength range of 300–1100 nm. The obtained results are shown in Figure 4.

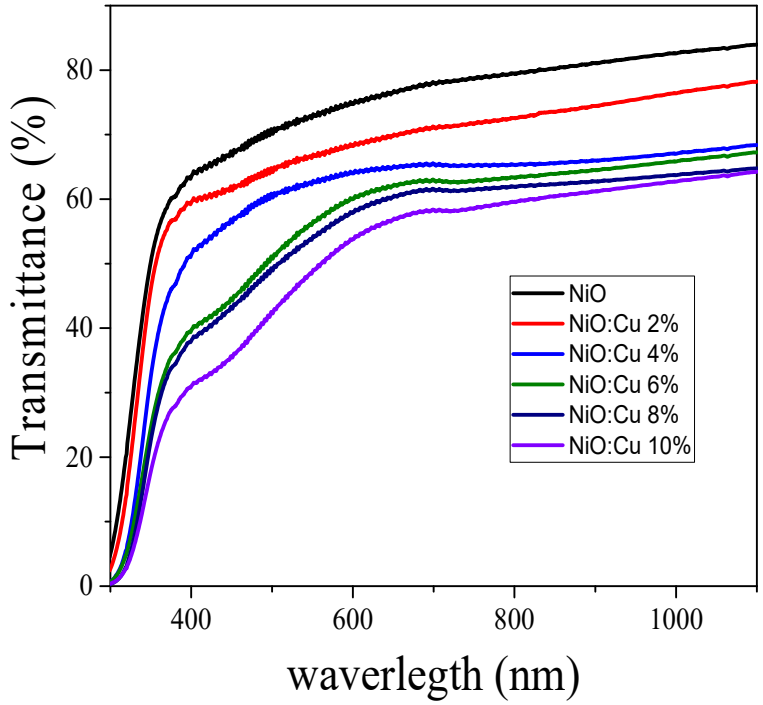

Figure 4. Transmittance spectra of pure and Cu-doping NiO films.

As it can be observed, the transmittance yield is around 70% for pure NiO films and is decreasing with increasing Cu-doping. We can split the transmittance spectra into two ranges: the first one at a wavelength lower than 400 nm for which transmittance is almost inexistent and where it exhibits the beginning of absorption owing to the direct transition between the valence and conduction bands. The second is at a wavelength greater than 400 nm showing the transparency of NiO films whose transmittance yield depends on Cu-doping concentration, in agreement with the literature where Mn, Zn, and Fe doping were used [44,45]. It is observed that with increasing Cu-doping, there is a decrease in transmittance and an increase in the absorbance attributed to changes in the crystalline structure due probably to the increase in NiO film thickness as indicated in XRD results. By combining the transmittance and absorption data and applying the Tauc's relation [46], we have estimated the values of the band gap E_g of NiO.

$$(\alpha h\nu)^2 = A(h\nu - E_g) \quad (6)$$

where α is the absorption yield, $h\nu$ is the photon energy, A is a constant, and E_g is the band gap energy.

E_g was obtained from the plot of Equation (6) by extrapolation the linear portion of the curve to $(\alpha h\nu)^2 = 0$ which intersects the energy axis (Figure 5).

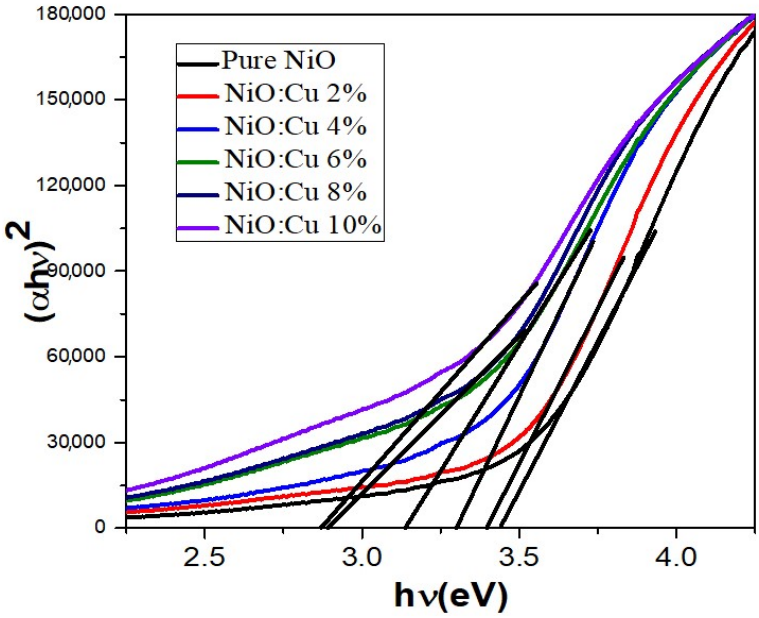

Figure 5. Plot of $(\alpha h\nu)^2$ vs. $h\nu$ for E_g gap estimation.

The obtained band gap values are presented in Table 4.

Table 4. Different values of band gap energy.

NiO	Band Gap (eV)	E_g Band Gap from Literature
NiO pure	3.450	3.085–3.116 [47] 3.6–4 [48] 3.83–3.14 [49]
NiO:Cu 2%	3.4051	
NiO:Cu 4%	3.2953	
NiO:Cu 6%	3.1373	
NiO:Cu 8%	2.8954	
NiO:Cu 10%	2.8648	

From Table 4, the band gap energy values are found in the range of E_g given in the literature [47–49]. Furthermore, the energy gap of Cu-doped NiO decreases with the increase in the grain size as discussed in SEM and AFM results. The decrease in E_g can be attributed to crystallinity improvement of deposited NiO films.

2.3. Photocatalytical Activity

The efficiency of photocatalytical activity to degradation of the organic pollutants by TCO nanoparticles are of increasing interest [50–53]. Photocatalytical activity describes a process whereby a semi-conductor nanomaterial such as NiO is excited by UV-radiation whose energy is equal to or larger than the band gap energy. The radiation is capable of catalyzing a redox reaction at its surface by creating a charge lying within the TCO band gap. Photocatalytic activity of the synthesized pure and Cu-NiO films was tested by the photodegradation of an aqueous solution of methylene blue. To do this, we introduced deposited NiO and Cu-NiO films in a solution of MB, and we measured its absorbance as a function of UV-irradiation time. We recorded the decrease in absorbance signal α after every 30 min. As it can be seen in Figure 6, the absorbance signal is composed of two peaks at around 613 and 664 nm.

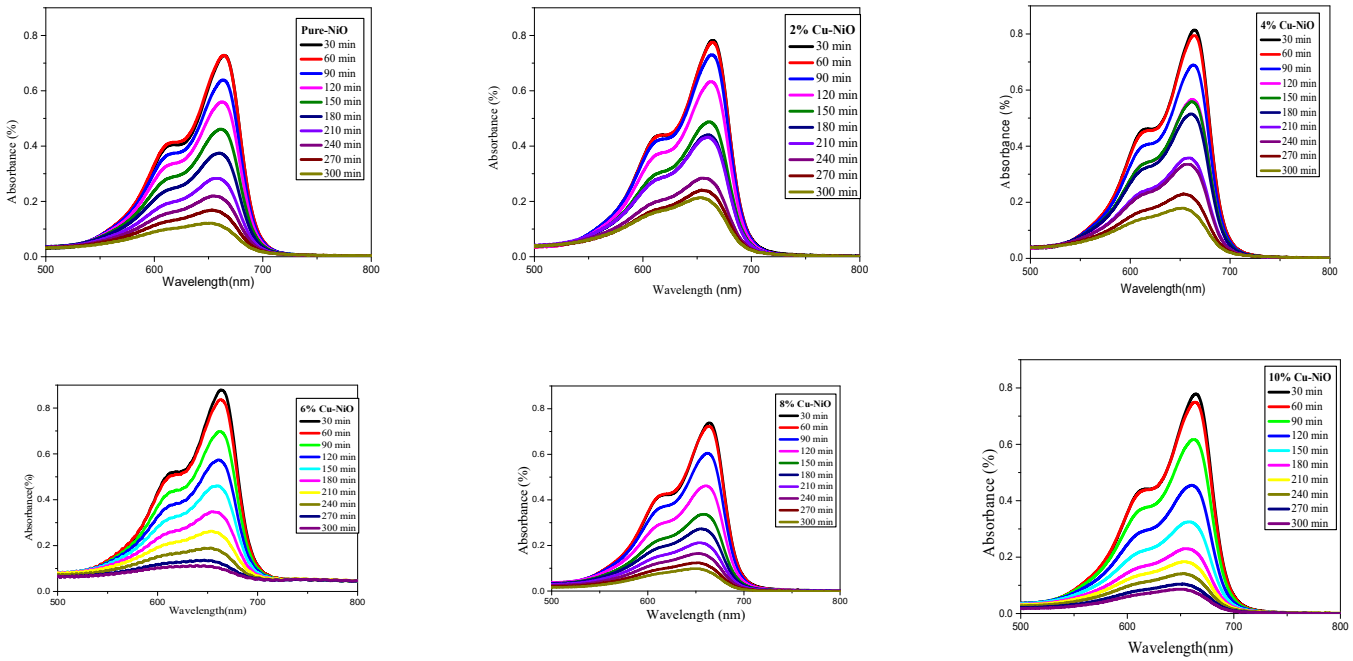

Figure 6. Effect of NiO nanoparticles on the decrease in Methylene Blue aqueous solution during UV irradiation.

The signal of the absorbance bands decreases during UV-irradiation time. The signal degradation is observed to be faster in the case where the Cu-doping is higher. The interpretation of these results may be explained in terms of electronic excitation processes.

The increase in the degradation rate of MB dye is attributed to the incorporation of Cu^{2+} in the lattice of NiO nanoparticles which reduces the electron–hole pair recombination and provides an increased number of free electrons and holes for the formation of free radical ions OH^{-}. During UV-illumination with a photocatalyst, the electron in the conduction band is photoactivated and is transferred to the valence band, creating an electron–hole pair capable of forming OH^{-} ions. These OH^{-} ions further combine with organic pollutant to produce final degraded products (Figure 7).

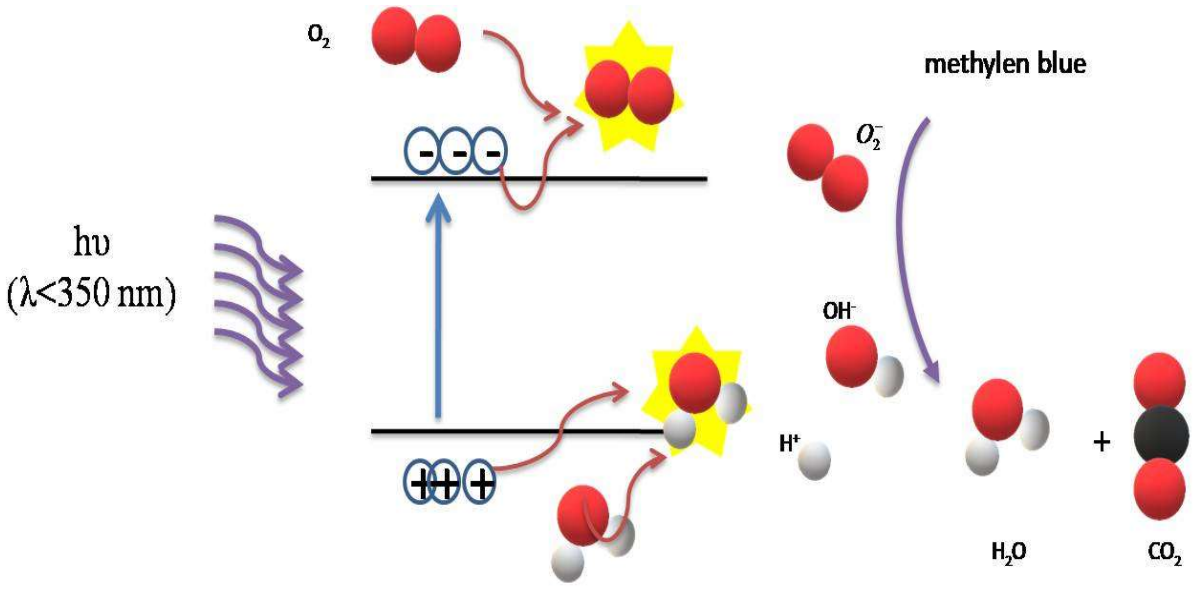

Figure 7. Schematic photodegradation diagram.

The reactions between holes and hydroxide groups produce O-H radicals and peroxide groups ($H_2O_2^-$). These radicals react with the MB solution dye and degrade it into non-toxic organic compounds. As discussed above, Cu-doping reduces NiO nanoparticle sizes and improves crystalline quality. NiO nanoparticles reduction is better with the increase in Cu-doping.

We suggest that small NiO particles combined with Cu-particles capture photons more efficiently and generate electron–hole pairs in larger quantities, and exhibit more and more photocatalytic activity. It is to be noted that the blue color of MB solution disappears after 300 min, especially for high Cu-doping (Figure 8).

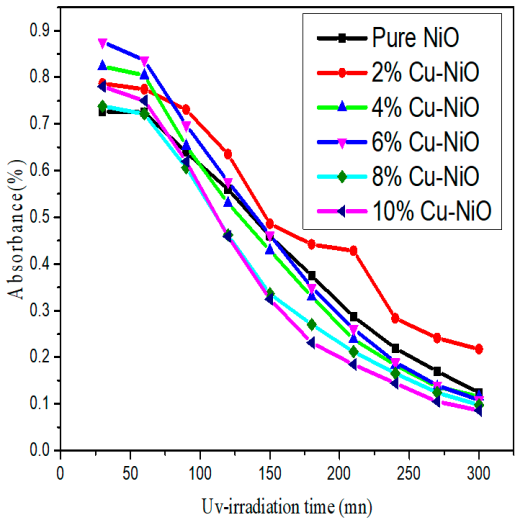

Figure 8. Degradation of the intensity of the absorption peak at 663 nm during UV-irradiation time.

As discussed in our previous work [54,55] and reported by Khan et al. [56,57], the photocatalysis carried out in atmospheric air show that the role of the nanoparticles of the films and of the oxygen O_2 is essential for the degradation of MB dye solution.

It is suggested that small NiO particles, capture photons more efficiently, generating electron–hole pairs in larger quantities and hence causing the more heavily doped NiO to exhibit a higher photocatalytic activity in the degradation of MB. The photocatalytic phenomenon can be explained in two steps:

(i) Step 1:

- During UV-light illumination, electrons are extracted from the valence band to the conduction band; electron–hole pairs are then created.
- O-H radicals and peroxide groups (O^{2-}) are produced by the presence of holes.
- The peroxides interact with the protons and form HO^{2-} and H_2O^{2-} species.

(ii) Step 2:

During UV-irradiation, the species present in MB solution interact with and degrade it. Step 1 and 2 can be displayed by the following mechanisms:

$$NiO + h\nu\ (uv) \rightarrow NiO + e^- + h^+ \quad (7)$$

$$H_2O \rightarrow OH^- + H^+ \quad (8)$$

$$OH^- + h^+ \rightarrow OH^* \quad (9)$$

$$O_2 + e^- \rightarrow O^-{}_2 \quad (10)$$

$$O_2{}^- + H^+ \rightarrow HO_2 \quad (11)$$

$$2HO_2 \rightarrow H_2O_2 + O_2 \quad (12)$$

$$H_2O_2 + e^- \rightarrow OH^- + OH^- \quad (13)$$

3. Materials and Method

Pure and copper-doped nickel oxide (NiO) thin films were deposited onto glass substrates heated at 400 °C using the spray pyrolysis method according to the following schema of Figure 9.

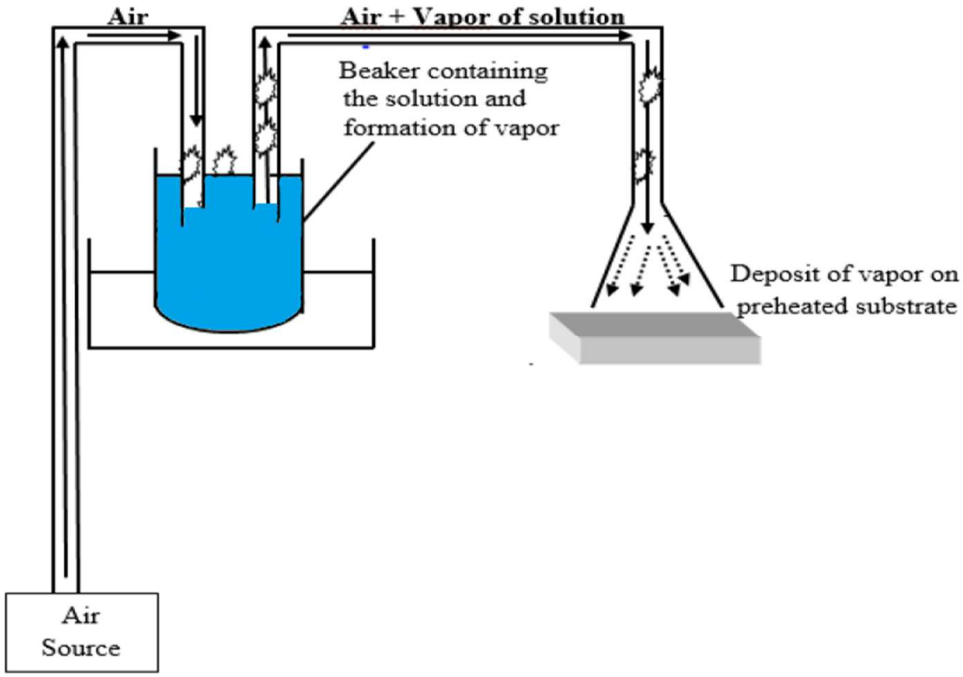

Figure 9. Principle schema of the spray pyrolysis technique.

Pure NiO was obtained from a primary solution of 0.2 M of nickel nitrate hexahydrate ($Ni(NO_3)_2$ $6H_2O$) dissolved in 100 mL distilled water. Copper-doping is obtained by adding a second solution prepared from copper nitrate hydrate ($Cu(NO_3)_3$ $9H_2O$) dissolved in distilled water at various concentrations of 2, 4, 6, 8, and 10% for obtaining Cu-doped NiO nanofilms. All precursor powders of purity of more than 98% were purchased from Biochem Chemopharma. All reagents were used as such without any further purification.

The obtained pure and Cu-doped samples were characterized by different techniques adapted to thin films analysis. X-ray diffraction (XRD) patterns were recorded to characterize films crystallinity and the phases using Panalytical X'Pert diffractometer with monochromatic high-intensity Cu-Kα radiation (λ = 0.1506 nm). Microstructural and morphological characterizations were obtained by scanning electron microscopy (SEM) (Hitashi instrument) and atomic force microscopy (AFM) (Bruker, Dimension Edge apparatus), respectively. The materials band gap energy (E_g) was extracted from the Tauc's plot, which combines absorption and transmittance data obtained from UV-visible spectroscopy analysis (Specord 50 plus).

Photocatalytical experiments were performed in a dark chamber where the beakers containing the Methylene blue (MB) solution and NiO and Cu-NiO samples were placed there. The whole was illuminated by a UV lamp of wavelength 253.7 nm.

4. Conclusions

Pure and Cu-NiO nanofilms were successfully synthesized by the spray pyrolysis method through a solution using nickel nitrate hexahydrate ($Ni(NO_3)_2 \cdot 6H_2O$) for NiO films and copper nitrate hydrate ($Cu(NO_3)_3 \cdot 9H_2O$) for Cu-doping NiO films. The aim of this study is to monitor the effect of Cu-doping on the structural, morphological, optical and photocatalytic properties. XRD, SEM, AFM, and UV-visible spectroscopy were used to characterize the synthesized samples. XRD revealed polycrystalline phases growing in cubic structure with (200) preferred orientation. SEM and AFM showed a rough surface

composed of spherical nanoparticles, which agglomerate with the increase in Cu-doping. Optical and photocatalytic properties investigated by UV-visible spectrometer showed that all NiO films are of good transparency, having a semiconducting character as revealed by the band gap energy ranging between 3.4450–2.8648 eV. The photocatalytic properties of pure and Cu-NiO films were enhanced by Cu-doping particles, as revealed by the degradation of methylene blue (MB) solution under ultraviolet irradiation. The bleaching of MB solution is faster for high Cu-doping, and it is correlated to the conductive behavior of NiO films.

Author Contributions: M.A. synthesized and characterized NiO samples; M.G. designed the study, supervised the results, and wrote the paper; M.A.D. performed the experiments and synthesized the results; A.B. participated in the interpretation of photocatalytical properties, D.B. revised the manuscript; D.T. contributed to the interpretations of optical results and took care of the article processing charge; C.F. participated to the explanation of XRD results. In general, all authors contributed to the preparation of this article. All authors have read and agreed to the published version of the manuscript.

Funding: This research was funded by DGRSDT-MESRS in the framework of the operating budget for PhD students 2019/2021 allocated to the "Laboratoire des Sciences de la Matière Condensée" (LSMC) and completed at the "Centre Interdisciplinaire de Nanosciences de Marseille" (CINaM). The authors would like to thank the French National Agency of Research (ANR) (project 'Nanoptix' # ANR-18-CE42-0016-02) for financial support.

Institutional Review Board Statement: Not applicable.

Informed Consent Statement: Not applicable.

Data Availability Statement: Data is contained within the article.

Conflicts of Interest: The authors declare no conflict of interest.

Sample Availability: Not applicable.

References

1. Kayan, Z.N.; Saleemi, F.; Batool, I. Synthesis and Characterization of ZnO Nanoparticles. *Mater. Today Proc.* **2015**, *2*, 5619–5621. [CrossRef]
2. Viana, M.M.; Soares, V.F.; Mohallem, N.D.S. Synthesis and Characterization of TiO_2 nanoparticles. *Ceram. Int.* **2010**, *36*, 2047–2053. [CrossRef]
3. Kumar, B.; Smita, K.; Debut, A.; Cumbal, L. Synthesis and characterization of SnO_2 nanoparticles using cochineal dye. *Appl. Phys. A* **2020**, *126*, 779. [CrossRef]
4. Renuga, D.; Jeyasundari, J.; Shakthi, A.A.S.; Brightson, A.J. Synthesis and characterization of copper oxide nanoparticles using Brassica oleracea var. italic extract for its antifungal application. *Mater. Res. Express* **2020**, *7*, 4. [CrossRef]
5. Bielz, T.; Lorenz, H.; Jochum, W.; Kaindl, R.; Klauser, F.; Kloetzer, B.; Penner, S. Hydrogen on In_2O_3: Reducibility, bonding, defect formation, and reactivity. *J. Phys. Chem. C* **2010**, *114*, 9022–9029. [CrossRef]
6. Golovanov, V.; Maki-Jaskari, M.A.; Rantala, T.T.; Korotcenkov, G.; Brinzari, V.; Cornet, A.; Morante, J. Experimental and theoretical studies of the indium oxide-based gas sensors deposited by spray pyrolysis. *Sens. Actuators B* **2005**, *106*, 563–571.
7. Fukano, T.; Motohiro, T. Low-temperature growth of highly crystallized transparent conductive fluorine-doped tin oxide films by intermittent spray pyrolysis deposition. *Sol. Energy Mater. Sol. Cells* **2004**, *82*, 567–575. [CrossRef]
8. Reyes-Herrera, J.; Acosta-Slane, D.; Castillo-Michel, H.; Pradas del Real, A.E.; Vogel-Mikus, K.; Benetti, F.; Roman, M.; Villanova, J.; Valles-Aragón, M.C. Detection and Characterization of TiO_2 Nanomaterials in Sludge from Wastewater Treatment Plants of Chihuahua State, Mexico. *Nanomaterials* **2022**, *12*, 744. [CrossRef]
9. Fereshteh, M.; Mozdianfard, M.R.; Soofivand, F.; Salavati-Niasari, M. NiO nanostructures: Synthesis, characterization and photocatalyst application in dye wastewater treatment. *RSC Adv.* **2014**, *4*, 27654–27660.
10. Herrmann, M.; Jansen, F.; van Santen, R.A. *Catalytic Science Series*; Imperial College Press: London, UK, 1999; pp. 171–180.
11. El-Hakam, S.A.; ALShorifi, F.T.; Salama, R.S.; Gamal, S.; El-Yazeed, W.A.; Ibrahim, A.A.; Ahmed, A.I. Application of nanostructured mesoporous silica/ bismuth vanadate composite catalysts for the degradation of methylene blue and brilliant green. *J. Mat. Res. Technol.* **2022**, *18*, 1963–1976. [CrossRef]
12. Sun, L.; Hu, D.; Zhang, Z.; Deng, X. Oxidative degradation of methylene blue via PDS-based advanced oxidation process usingnatural pyrite. *Int. J. Environ. Res. Public Health* **2019**, *16*, 4773. [CrossRef] [PubMed]

13. Cheng, J.; Zhan, C.; Wu, J.; Cui, Z.; Si, J.; Wang, Q.; Peng, X.; Turng, L.S. Highly Efficient Removal of Methylene Blue Dye from anAqueous Solution Using Cellulose Acetate Nanofibrous Membranes Modified by Polydopamine. *ACS Omega* **2020**, *5*, 5389–5400. [CrossRef] [PubMed]
14. Dharmraj Khairnar, S.; Shankar Shrivastava, V. Facile synthesis of nickel oxide nanoparticles for the degradation of Methylene blue and Rhodamine B dye: A comparative study. *J. Taibah Univ. Sci.* **2019**, *13*, 1108–1118. [CrossRef]
15. Mannaa, M.A.; Qasim, K.F.; Alshorifi, F.T.; El-Bahy, S.M.; Salama, R.S. Role of NiO Nanoparticles in Enhancing Structure Properties of TiO_2 and Its Applications in Photodegradation and Hydrogen Evolution. *ACS Omega* **2021**, *6*, 30386–30400. [CrossRef]
16. Sabouri, Z.; Fereydouni, N.; Akbari, A.; Ali Hosseini, H.; Hashemzadeh, A.; Sadegh Amiri, M.; Kazemi Oskuee, R.; Darroudi, M. Plant-based synthesis of NiO nanoparticles using salvia macrosiphon Boiss extract and examination of their water treatment. *Rare Met.* **2020**, *39*, 1134–1144. [CrossRef]
17. Manouchehri, I.; Mehrparvar, D.; Moradian, R.; Gholami, K.; Osati, T. Investigation of structural and optical properties of copper doped NiO thin films deposited by RF magnetron reactive sputtering. *Optik* **2016**, *127*, 8124–8129. [CrossRef]
18. Gandhi, A.C.; Yun Wu, S. Strong Deep-Level-Emission Photoluminescence in NiO Nanoparticles. *Nanomaterials* **2017**, *7*, 231. [CrossRef]
19. Shang, Z.W.; Hsu, H.H.; Zheng, Z.W.; Cheng, C.H. Progress and challenges in p-type oxide-based thin film transistors. *Nanotechnol. Rev.* **2019**, *8*, 422–443. [CrossRef]
20. Hotovy, I.; Spiess, L.; Predanocy, M.; Rehacek, V.; Racko, J. Sputtered nanocrystalline NiO thin films for very low ethanol detection. *Vacuum* **2014**, *107*, 129–131. [CrossRef]
21. Korosec, R.C.; Bukovec, P. Sol-gel preparation NiO thin films for electrochromic applications. *Acta Chim. Slov.* **2006**, *53*, 136–147.
22. Garcia-Garcia, F.J.; Salazar, P.; Yubero, F.; González-Elipe, A.R. Non-enzymatic glucose electrochemical sensor made of porous NiO thin films prepared by reactive magnetron sputtering at oblique angles. *Electrochim. Acta* **2016**, *201*, 38–44. [CrossRef]
23. Mironova-Ulmane, N.; Kuzmin, A.; Sildos, I.; Puust, L.; Grabis, J. Magnon and Phonon Excitations in Nanosized NiO. *Latv. J. Phys. Tech. Sci.* **2019**, *56*, 61–72. [CrossRef]
24. Reddy, A.M.; Reddy, A.S.; Lee, K.S.; Reddy, P.S. Growth and characterization of NiO thin films prepared by dc reactive magnetron sputtering. *Solid. Stat. Sci.* **2011**, *13*, 314–320. [CrossRef]
25. Bahramian, A.; Eyraud, M.; Vacandio, F.; Hornebecq, V.; Djenizian, T.; Knauth, P. Single-step electrodeposition of superhydrophobic black NiO thin films. *J. Appl. Electrochem.* **2018**, *49*, 621–629. [CrossRef]
26. Khalaf, M.M.; Hany, M.; El-Lateef, A. Corrosion protection of mild steel by coating with TiO2 thin films co-doped with NiO and ZrO2 in acidic chloride environments. *Mater. Chem. Phys.* **2016**, *177*, 250–265. [CrossRef]
27. Dahamni, M.A.; Ghamnia, M.; Naceri, S.E.; Fauquet, C.; Tonneau, D.; Pireaux, J.-J.; Bouadi, A. Spray Pyrolysis Synthesis of Pure and Mg-Doped Manganese Oxide Thin Films. *Coatings* **2021**, *11*, 598. [CrossRef]
28. Benameur, N.; Chakhoum, M.A.; Boukhachem, A.; Dahamni, M.A.; Ghamnia, M.; Hacini, N.; Pireaux, J.P.; Houssiau, L.; Ziouche, A. Investigation of some physical properties of pure and Co-doped MoO3 synthesized on glass substrates by the spray pyrolysis method. *J. Electron Spectrosc. Relat. Phenom.* **2019**, *234*, 79–97. [CrossRef]
29. Ouhaibi, A.; Ghamnia, M.; Dahamni, M.A.; Heresanu, V.; Fauquet, C.; Tonneau, D. The effect of Strontium doping on structural and morphological properties of ZnO nanofilms synthesized by ultrasonic spray pyrolysis method. *J. Sci. Adv. Mater. Devices* **2018**, *36*, 29–36. [CrossRef]
30. Kooti, M.; Jorf, M. Synthesis and characterization of nanosized NiO_2 and NiO using Triton X-100. *Cent. Eur. J. Chem.* **2009**, *7*, 155–158. [CrossRef]
31. AL-Rashedi, K.; Farooqui, M.; Rabbani, G. Nickel Oxide Thin Film Synthesis by Sol-Gel Method on Glass Substrates. *Int. J. Univers. Print* **2018**, *4*, 508–516.
32. Alver, U.; Yaykaşl, H.; Kerli, S.; Tanrıverdi, A. Synthesis and characterization of boron-doped NiO thin films produced by spray pyrolysis. *Int. J Miner. Metall. Mater.* **2013**, *20*, 1097–1101. [CrossRef]
33. Chen, S.C.; Kuo, T.Y.; Lin, Y.C.; Lin, H.C. Preparation and properties of p-type transparent conductive Cu-doped NiO films. *Thin Solid Films* **2011**, *519*, 4944–4947. [CrossRef]
34. Gowthami, V.; Meenakshi, M.; Anandhan, N.; Sanjeeviraja, C. Preparation of Cu-doped Nickel Oxide Thin Films and their Properties. *AIP Conf. Proc.* **2014**, *1591*, 884. [CrossRef]
35. Cullity, B.; Stock, S. *Principles of XRay Diffraction*; Addison Wesley: Boston, MA, USA, 1978.
36. Vijaya Kumar, P.; Jafar Ahamed, A.; Karthikeyan, M. Synthesis and characterization of NiO nanoparticles by chemical as well as green routes and their comparisons with respect to cytotoxic effect and toxicity studies in microbial and MCF-7 cancer cell models. *SN Appl. Sci.* **2019**, *1*, 1083. [CrossRef]
37. Nid, A.; Zighed, L.; Aoun, Y.; Maaoui, B. Synthesis and Characterization of Al-doped NiO Nanostructured Thin Films Elaborated by Solar Spray Pyrolysis Technique, for Photovoltaic Cells. *Preprints* **2021**, 2021110572. [CrossRef]
38. Mezher, J.S.; Dawood, M.O.; Beddai, A.A.; Mejbel, M.K. NiO nanostructure by RF sputtering for gas sensing applications. *Mater. Technol.* **2020**, *35*, 60–68. [CrossRef]
39. Borchert, H.; Shevchenko, E.V.; Robert, A.; Mekis, I.; Kornowski, A.; Grubel, G.; Weller, H. Determination of nanocrystalsizes: Comparison of TEM; SAXS and XRD studies of highly monodisperse CoPt3 particles. *Langmur* **2005**, *21*, 1931–1936. [CrossRef]
40. Habtea, A.G.; Honea, F.G.; Dejene, F.B. The influence of malonic acid on the structural, morphological and optical properties of CdSe thin films prepared by chemical bath deposition method. *Inorg. Chem. Commun.* **2019**, *103*, 107–112. [CrossRef]

41. Guo, F.; Yang, B.; Yuan, Y.; Xiao, Z.; Dong, Q.; Bi, Y.; Huang, J. A nanocomposite ultraviolet photodetector based on interfacial trap-controlled charge injection. *Nat. Nanotechnol.* **2012**, *7*, 798–802. [CrossRef]
42. Awais, M.; Rahman, M.; Don MacElroy, J.M.; Coburn, N.; Dini, D.; Vos, J.G.; Dowling, D.P. Deposition and characterization of NiO x coatings by magnetron sputtering for application in dye-sensitized solar cells. *Surf. Coat Technol.* **2010**, *204*, 2729–2736. [CrossRef]
43. Reddy, R.S.; Sreedhar, A.; Reddy, A.S.; Uthanna, S. Effect of film thickness on the structural morphological and optical properties of nanocrystalline ZnO films formed by RF magnetron sputtering. *Adv. Mater. Lett.* **2012**, *3*, 239–245. [CrossRef]
44. Ramesh, M. N and Fe doped NiO nanoparticles for enhanced photocatalytic degradation of azo dye methylene blue in the presence of visible light. *SN Appl. Sci.* **2021**, *3*, 817. [CrossRef]
45. Al Boukhari, J.; Zeidan, L.; Khalaf, A.; Awad, R. Synthesis, characterization, optical and magnetic properties of pure and Mn, Fe and Zn doped NiO nanoparticles. *Chem. Phys.* **2019**, *516*, 116–124. [CrossRef]
46. Tauc, J. *Amorphous and Liquid Semiconductors*; Springer: Boston, MA, USA, 1974; p. 159.
47. Rahal, H.T.; Awad, R.; Abdel-Gaber, A.M.; El-Said Bakeer, D. Synthesis, Characterization, and Magnetic Properties of Pure and EDTA-Capped NiO Nanosized Particles. *J. Nanomater.* **2017**, *2017*, 7460323. [CrossRef]
48. Chen, X.; Zhao, L.; Niu, Q. Electrical and optical properties of p-type Li, Cu-codoped NiO thin films. *J. Electron. Mater.* **2012**, *41*, 3382–3393. [CrossRef]
49. Safwat Mahmoud, A.; Alshomer, S.; Tarawnh, A.M. Structural and Optical Dispersion Characterisation of Sprayed Nickel Oxide Thin Films. *J. Mod. Phys.* **2011**, *2*, 1178–1186. [CrossRef]
50. Boulila, S.; Ghamnia, M.; Boukhachem, A.; Ouhaibi, A.; Chakhoum, M.A.; Fauquet, C.; Heresanu, V.; Tonneau, D. Photocatalytical properties of NiO nanofilms doped with Ba. *Philos. Mag. Lett.* **2020**, *110*, 283–293. [CrossRef]
51. Chakhoum, M.A.; Bouchakhoum, A.; Ghamnia, M.; Benameur, N.; Mehdi, N.; Raouadi, K.; Amlouk, M. An attempt to study (111) oriented NiO-like TCO thin films in terms of structural, optical properties and photocatalytic activities under strontium doping. *Spectrochim. Acta Part A* **2018**, *205*, 649–660. [CrossRef]
52. Zhao, B.; Ke, X.K.; Bao, J.H.; Wang, C.L.; Dong, L.; Chen, Y.W.; Chen, H.L. Synthesis of Flower-Like NiO and Effects of Morphology on Its Catalytic Properties. *J. Phys. Chem. C* **2009**, *113*, 14440–14447. [CrossRef]
53. Karthikeyan, V.; Padmanaban, A.; Dhanasekaran, T.; Praveen Kumar, S.; Gnanamoorthy, G.; Narayanan, V. Synthesis and Characterization of ZnO/NiO and Its Photocatalytic Activity. *Photobiology* **2017**, *9*, 824–831.
54. Benameur, N.; Boukhachem, A.; Ghamnia, M.; Chakhoum, M.A.; Dahamni, M.A.; Fauquet, C. Investigation of Some Physical Properties of Cobalt Doped MoO_3 Nanofilms and Their Effects on the Degradation of the Methylene Blue Solution under UV Illumination. *Int. J. Chem. Eng. Appl.* **2019**, *10*, 33–39. [CrossRef]
55. Aroussi, S.; Dahamni, M.A.; Ghamnia, M.; Tonneau, D.; Fauquet, C. Characterization of Some Physical and Photocatalytic Properties of CuO Nanofilms Synthesized by a Gentle Chemical Technique. *Condens. Matter* **2022**, *7*, 37. [CrossRef]
56. Khan, I.; Saeed, K.; Zekker, I.; Zhang, B.; Hendi, A.H.; Ahmad, A.; Ahmad, S.; Zada, N.; Ahmad, H.; Shah, L.A.; et al. Review on Methylene Blue: Its Properties, Uses, Toxicity and Photodegradation. *Water* **2022**, *14*, 242. [CrossRef]
57. Khan, I.; Saeeda, K.; Alib, N.; Khanc, I.; Zhangd, B.; Sadiq, M. Heterogeneous photodegradation of industrial dyes: An insight to different mechanisms and rate affecting parameters. *J. Environ. Chem. Eng.* **2020**, *8*, 104364. [CrossRef]